Construction and Design of Diffractive Optical Elements with Nanoscale Features

Benjamin Ranson

*Physics & Astronomy Department, University of South Carolina.**

(Dated: April 25, 2022)

Contemporary thermal scanning-probe lithography (t-SPL) techniques can achieve patterning resolutions of 1 nanometer, on the order necessary to directly fabricate kinoform diffractive optical elements (DOEs) of arbitrary shape. These wavefront-modulating surfaces have immense potential to greatly decrease the form-factor of optical systems and thereby create many emergent applications. Here, using an adaptation of Gerchberg and Saxton's (1972) algorithm, a target far-field pattern is selected and an iterative 2D Fourier transforms to generated the needed relief structure, with an eye towards experimental fabrication and measurement with the SmartState Center's own t-SPL device, the Heidelburg Instruments NanoFrazor.

CONTENTS

* For source code or other questions: bengr444@gmail.com

Part I

Introduction

I. SUMMARY

In this paper, we model a diffractive optical system by means of a series of complex, 2D wavefront fields. We trace the relations between the elements in order to understand how a target image field could be produced by such a system consisting of a laser and a surface-relief diffractive optical element called a kinoform. We attempt to find solutions to this system and discuss the limitations of various algorithms and assumptions. Finally, we examine some computational results and discuss the feasibility of fabricating their corresponding kinoforms.

II. MOTIVATION

T. Crawford's self-assembling magnetic nanoparticle system has the necessary resolution to rapidly create detailed 2D diffractive gratings in the visible spectrum.[1] USC's own SmartState Center's Heidelburg Instrument NanoFrazor can use thermal scanning probe lithography to produce sub-nanometer resolution relief patterns which could be used to study potential patterns made with those nanoparticles. This paper introduces a model and the associated problems of a system created by a *Diffractive Optical Element* (DOE), specifically for DOEs of a class which could be fabricated using the NanoFrazor. The resulting analysis will serve as a launching point for further investigation into both kinds of aforementioned fabrication.

Part II

Problem Model

III. DIFFRACTIVE OPTICAL SYSTEM

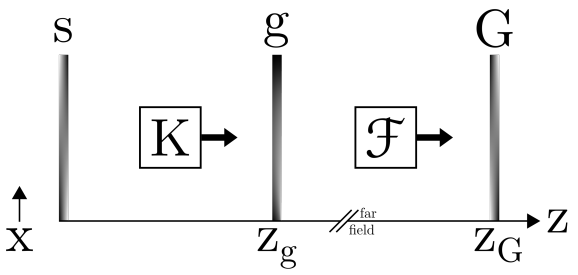

FIG. 1. Sequential process of the class of diffractive optical systems studied here. The y-axis is not shown.

The system consists of a source of illumination, a DOE, and a far-field image produced by their combination, arranged in 3-dimensional space. The system elements need not be axis-aligned, but for the sake of simplicity, here we will assume they are aligned along the z-axis.

We examine this system as a series of wavefronts, each one represented by a 2D field of complex numbers defined over (x, y). First, the source of illumination, s, located at $z = 0$. Secondly, the field after the DOE, g, located at $z = z_g$. Thirdly, the far-field image of the system, G, located at z_G. Each value in the fields represent the state of their respective wavefront as follows, using g as an example:

The amplitude, or modulus of $g = |g(x, y)|$,
The phase of g = $\phi\, g(x, y)$,

$$\phi\, g(x, y) = \arctan\left(\frac{\operatorname{Im} g(x, y)}{\operatorname{Re} g(x, y)}\right).$$

.

We will omit (x, y) for brevity or when referring to the field as a whole: for example,

consider the relations between the fields as we have defined them:

$$g = K(s),$$
$$G = \mathcal{F}(g).$$

A great utility of modeling wavefronts this way is that they can be decomposed into their phase and modulus through only multiplication:

$$g = |g| \cdot \exp i\,\phi\, g.$$

If g were to be transformed by having its amplitude halved and its phase advanced by π, then this operation could be modeled only with multiplication as well:

$$g' = g \cdot \frac{1}{2} \exp i\pi = \frac{|g|}{2} \cdot \exp(i\,\phi\, g + i\pi).$$

IV. THE KINOFORM AND LASER

Since we intend to physically fabricate the system, the fields s, g, and consequently G are not just theoretical tools, but are constrained to the available means and techniques.

With the ability to create a continuously-varying relief surface with the NanoFrazor, we choose our DOE to be a *kinoform*. A kinoform is a physical surface that either transmits or reflects light, altering the phase of incident light pointwise according to the physical depth or height of the kinoform's surface.[2] Kinoforms differ from similar DOEs in that their surface relief varies continuously, although the name sometimes refers to quantized approximations of such an element as well. For our model, we will consider a transmissive kinoform, but the same principles hold for a reflective one.

An important restriction on kinoforms is that they may only alter the amplitude of the light by decreasing it homogeneously, i.e. if the modulus of the incident light is lowered by passing through the kinoform, it is lowered by the same factor across its entire wavefront. Therefore the effect of any kinoform is only its ability to alter phase, up to a proportionality factor. For this reason, we will assume our kinoform has no effect on the amplitude of light transmitted through it.

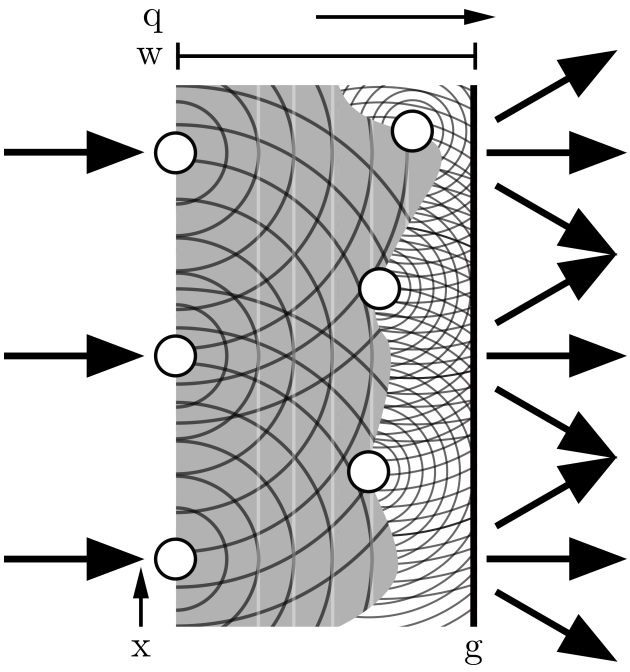

FIG. 2. The effect of a kinoform on a wavefront.

The phase-altering ability of a kinoform is granted by its depth, q, which varies as a function of (x, y), up to a maximum w.

In an equivalent empty region of space, the phase of the wavefront advances by kw, where $k = 2\pi/\lambda$, the angular wave-number of the wavefront. Passing through the kinoform advances the phase by $kqn + k(w - q)$, where n is the index of refraction of the kinoform medium. Therefore the relative advancement of the phase due to the kinoform is given by

$$\Delta\phi(x, y) = k(n - 1)q(x, y).$$

Phase advancements are only meaningful up to modulo 2π, which allows us to constrain $\Delta\phi \leq 2\pi$. The physical kinoform can therefore be constrained as

$$q(x, y) \leq \frac{\lambda}{n - 1}.$$

Since most widely available media tend to have $n \lessapprox 5$, the necessary depth of the kinoform is, in the worst case, on the order of

magnitude of the wavelength of its illuminating light. For visible light in the 400 nm to 700 nm spectrum, the worst cases pose a challenge to the NanoFrazor due to its limited cutting-depth.

The field g can be conceptualized as being located directly after the kinoform in z-order. The field g is determined by both the kinoform and the nature of the kinoform's illumination. Since the kinoform has no effect on the amplitude of s, the simplest division would be to make ϕg only a function of the kinoform, and $|g|$ only a function of the illumination on the kinoform, s. This is only achievable if all light incident on the kinoform is in phase. In addition, the operation of the kinoform requires all incident light to be of an equal wavelength. Therefore, s must be a monochromatic, coherent source of light, in practice provided by a laser.

Under the assumption that the distance between the kinoform and the laser, z_g, is small compared to the coherence length of the laser, we can now characterize the action of K as

$$\begin{aligned} g &= K(s), \\ g(x,y) &= K(s)(x,y), \\ &= |s(x,y)| \cdot \exp i\Delta\phi, \\ &= |s(x,y)| \cdot \exp\big(ik(n-1)q(x,y)\big). \end{aligned} \tag{1}$$

In effect, K represents propagation of s through the kinoform.

V. FRAUNHOFER DIFFRACTION

The field g serves as a source of spherical wavefronts each with wavelength λ, intensity $|g(x,y)|^2$, and phase $\phi g(x,y)$[1]. The interference of these waves produces a new field at each z-position, which converges as z goes to infinity, i.e. the far-field. In this regime, the resulting diffraction pattern is described by Fraunhofer diffraction. A converging lens will also produce an equivalent diffraction pattern at its focal point. We let $\mathcal{F}\,g$ represent this far-field propagation, and G is the far-field wavefront.

It has been shown[3] that

$$\begin{aligned} G(u,v) &= (\mathcal{F}\,g)(u,v), \\ &= \iint_{-\infty}^{+\infty} g(x,y) \exp\big(i(ux+vy)\big)dxdy, \\ &= \text{Continuous Fourier-transform of g} \end{aligned}$$

Therefore we can characterize the action of $\mathcal{F}$ as

$$\mathcal{F} = \text{Continuous Fourier-transform.}$$

The field G exists in space and as such (u,v) represents a spatial location that can be expressed in terms of our coordinate system as

$$u = \frac{x}{\lambda\Delta z}, v = \frac{y}{\lambda\Delta z},$$

where $\Delta z = z_G - z_g$, the distance between g and G.

Since $\mathcal{F}$ is the Fourier-transform, $\overline{\mathcal{F}}$, its unique inverse, exists, and can be used to find g for a particular, concrete G.

VI. PHASE-RETRIEVAL AND UNDERSPECIFICATION

For the design of a kinoform, we first select a desired visible image for the kinoform to produce. To many optical systems as well as the naked eye, only the intensity, $|G|^2$ is relevant, and thus it defines what is the visible image. Furthermore, in some problems, any image of intensity proportional to $|G|^2$ will also suffice; ours is one such problem.

Clearly, g cannot be found merely from $|G|^2$ or $|G|$, since the inverse propagation, $\overline{\mathcal{F}}$, needs a phase-component of G to be specified. In effect, G is *underspecified*. This is

[1] The small, conventional approximation that all pointlike light-sources resulting from the action of the kinoform are located at the same z-position is made here and is fully justified by the far-field limiting process.

the defining issue of the problem of *phase-retrieval*.[4]

In the phase-retrieval problem, the principle goal is to recover $\phi\, G$ by making assumptions about the constraints of G from knowledge of the physical system. In our problem, we are agnostic to $\phi\, G$; it remains a free variable, but one that works in our favor. It has been noted that, in some sense, the phase of a wavefront "carries the majority of the information in [the] signal"[5]. Since we do not specify the phase, we, in effect, leave most of our variables in G unspecified.

Furthermore, we do not wish for the image of the system to be dependent on the exact nature of s. We do not wish to assume a particular spatial profile for our laser. A Gaussian profile, a uniform cylinder, or similar ought to all produce a facsimile of $|G|^2$.

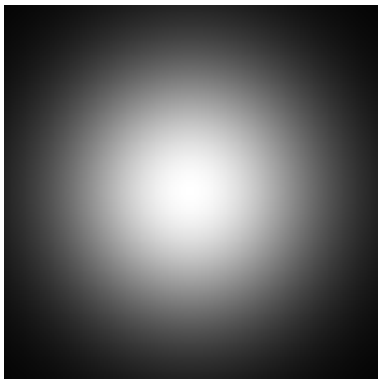

FIG. 3. Typical Gaussian amplitude (square-root of intensity) profile of a laser.

Due to the nature of the Fourier-transform, we require our illumination to be, in some sense, 'central', i.e. provide sufficient relative illumination on the centrally-located (x, y) positions of our kinoform, but otherwise we impose no further restrictions on it.

We summarize our specified and free variables as in table I.

$\lvert s\rvert$	A central distribution, but otherwise unknown.
$\phi\, s$	Equal over all (x, y).
q	Independent, free choice. We wish to select this to produce our choice of image.
K	Fully specified by the combination of q and $\lvert s\rvert$.
$\lvert g\rvert$	Equal to $\lvert s\rvert$.
$\phi\, g$	Determined only by q.
$\mathcal{F}$	Fully specified by nature of Fraunhofer diffraction.
$\lvert G\rvert$	Independent, free choice.
$\phi\, G$	Independent choice with no effect on solutions.

TABLE I. Table of specified and free variables in our optical system.

We now introduce a tool to help us find q. Let $g^\star$ be a wavefront that satisfies

$$|g^\star| = 1,$$
$$\phi\, g^\star = \phi\, g.$$

i.e.

$$g^\star = |1| \cdot \exp i\, \phi\, g,$$

It must then be the case that

$$g(x, y) = |s(x, y)| \cdot g^\star(x, y). \tag{2}$$

The only difference between g and $g^\star$ would be the choice of illumination. With this in mind, examining table I informs us that by finding $g^\star$ for the system, we effectively also find q, while remaining agnostic to the choice of s.

Unfortunately, there exists no analytic method to find a field satisfying these constraints. To take just one example, $\overline{\mathcal{F}}G$ certainly does not generally satisfy the condition $|\overline{\mathcal{F}}G| = 1$ for an arbitrary $|G|$.

Part III

Computational Solution

VII. SETUP

When analytic methods fail, the physicist's favorite tool is numerical methods.

We specify our digitized image, $|G'_0|$ as a $N \times N$ matrix of floating-point values proportional to our target image, $|G|$, sampled uniformly.

In place of the inapplicable continuous Fourier-transform, we let $\mathcal{F}$ be the discrete 2D *fast-Fourier transform* (FFT)[6], which generates a equally-sized matrix of frequencies and their corresponding amplitudes from the input, represented, as in the continuous case, as complex values. Up to a circular shift, this matrix corresponds to g'_0, the wavefront field which would propagate to G'_0. We inherit the continuous Fourier-transform's need of a phase to be specified for G'_0.

VIII. THE GERCHBERG-SAXTON ALGORITHM

R. Gerchberg and W. Saxton's 1971 technique[7] served as the basis for most future attempts to use iterated Fourier-transforms to solve the phase-retrieval problem in the field of computer-generated holography. Here, we adapt it to finding the optimal design for our kinoform. The algorithm is described schematically in figure 4.

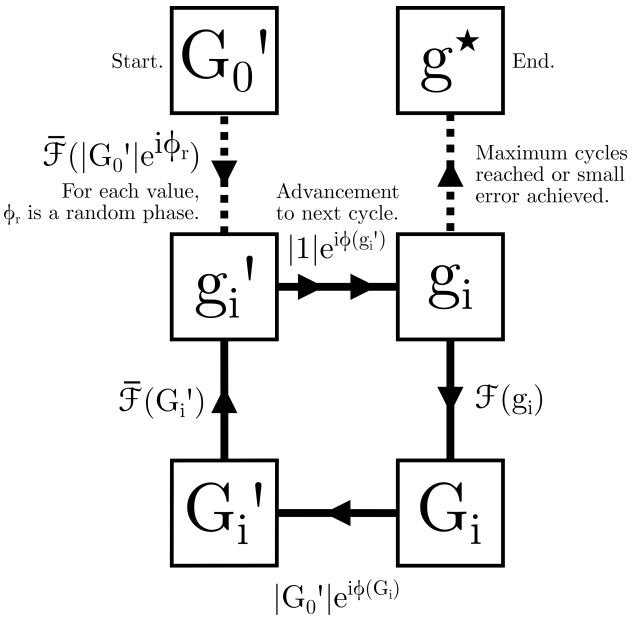

FIG. 4. The Gerchberg-Saxton algorithm. Each node is equal to the process described by the arrow leading into it.

The algorithm as adapted to our problem is as follows: the target image to be produced, $|G'_0|$ is taken as an input. It is assigned random phase values for each of its cells. It is then inverse-Fourier-transformed to produce g'_0.

The setup completed, the algorithm repeats the following cycle: g'_{i-1} is modified in the simplest manner to satisfy all object-field constraints, producing g_i, a guess for the object-field. The guess is then Fourier-transformed to produce G_i, which does not necessarily resemble the original target image. G'_i is the correction of G_i, produced by keeping $\phi\, G_i$, but setting its moduli to match the original image, $|G'_0|$. Finally, G'_i is reverse-Fourier-transformed into g'_i, terminating the cycle.

As shown in figure 4, our image constraints are that $|G_i| = |G'_0|$, as is standard, and our object constrains demand that $|g_i| = 1$.

If the error between G_i and G'_0 is small enough, or the maximum number of cycles is achieved, the algorithm stops, and g_i is kept as $g^\star$, which can be used to design the kino-

form.

The mean-squared error (MSE) serves as a measure of the produced image's (G_i) difference from the target image ($|G'_0|$), and is calculated as

$$\mathrm{MSE}_i = \frac{\sum |G_i - G'_i|^2}{\sum |G'_i|^2},$$

where the sums are over all matrix elements.

It has been shown that the MSE necessarily decreases with each iteration for most applications.[7] Despite this, there are a number of powerful objections to the algorithm. There is no guarantee the error goes to zero, merely that it decreases. In our trials, the error merely converged to a fixed value. Secondly, There is no guarantee that a solution exists for any object-field (g) or image-field (G) constraints. The rate at which the error decreases depends on the initial setup. Since the initial phases for G'_0 are random, the algorithm is stochastic.

Finally, the algorithm attempts to finds a locally-optimal solution, not a globally-optimal one: there may exist a g_i whose image has lower MSE, but since it does not exist along the algorithms 'descent-path', it cannot be found. There is also no technique to know whether another solution may exist which is more optimal, except, perhaps, visual intuition.

IX. FIENUP'S INPUT-OUTPUT ALGORITHM

Based on the Gerchberg-Saxton algorithm, J. Fienup developed a number of algorithms dubbed 'input-output' algorithms.[8, 9] The "Hybrid" input-output algorithm stands as the practical industry standard for solving phase-retrival problems.[5]

These algorithms treated the $G_i \to G'_i$ 'side' of the algorithm as a semilinear blackbox. The task at hand was viewed not as iterative corrections to guesses in the two domains, but instead to generate a g_i whose corresponding g'_i would already closely satisfy the object constraints before corrections.

We have chosen not to use any variation of Fienup's algorithm because they provide no additional benefit to our case, and often reduce to be nearly identical. See appendix A for more details.

X. RESULTS

In general, the algorithm converged extremely quickly to a locally-optimal solution with significant remaining MSE. Other than this, there were no problems enforcing the condition that $|g^\star| = 1$, ignoring floating-point rounding errors.

XI. QUANTIZED DIFFRACTIVE OPTICAL ELEMENTS

The aforementioned nanoparticle system will likely only only be able to create what are known as binary holograms. These DOEs, (which we let correspond to $h^\star$) consist of only two phase-levels, but otherwise satisfy all other properties of $g^\star$. By treating the two-level condition as an additional object-field constraint, we can use our algorithm to also design these.

For each $H'_{i-1}(u, v)$, if the phase is less than 0, then the corresponding element of H_i has its phase set to 0, otherwise the phase is set to $+\pi$.

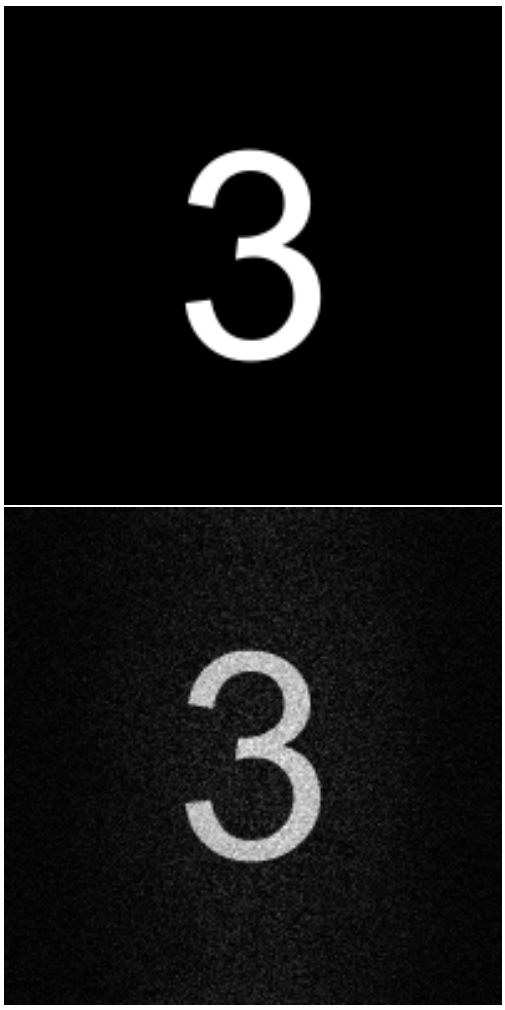

FIG. 5. Top: picture of the number '3'.
Bottom: $|G_5|$, the image reconstruction after 5 iterations. No further significant reduction in error for subsequent iterations. Note the visible noise's horizontal dependence.

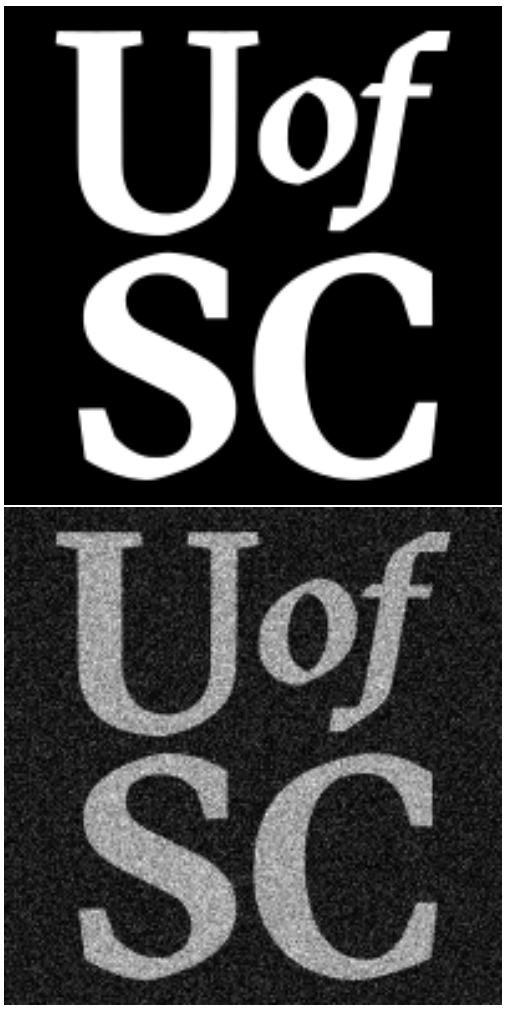

FIG. 6. Top: the UofSC logo.
Bottom: $|G_5|$, the image reconstruction after 5 iterations. No further significant reduction in error for subsequent iterations. Note the significant visual noise in the area which should be black.

FIG. 7. Top: Photo of a cat (from the Wikimedia Commons).
Bottom: $|G_5|$, the image reconstruction after 5 iterations. No further significant reduction in error for subsequent iterations.

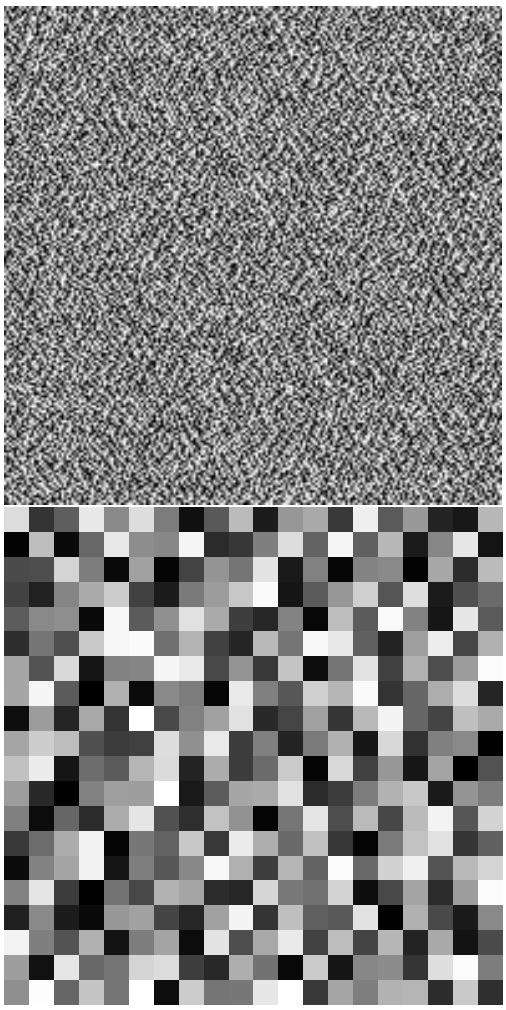

FIG. 8. Top: Final phases, $\phi\, g_5$, for the image in figure 6. The matrix has been circularly-rolled so the phases corresponding to the lowest frequencies appear in the center.
Bottom: 200 of the lowest-frequency phases (taxicab distance).

FIG. 9. The moduli, $|H_5|$ of figure 6 resulting from a binary DOE. It appears as two copies of the target image, one doubly-inverted.

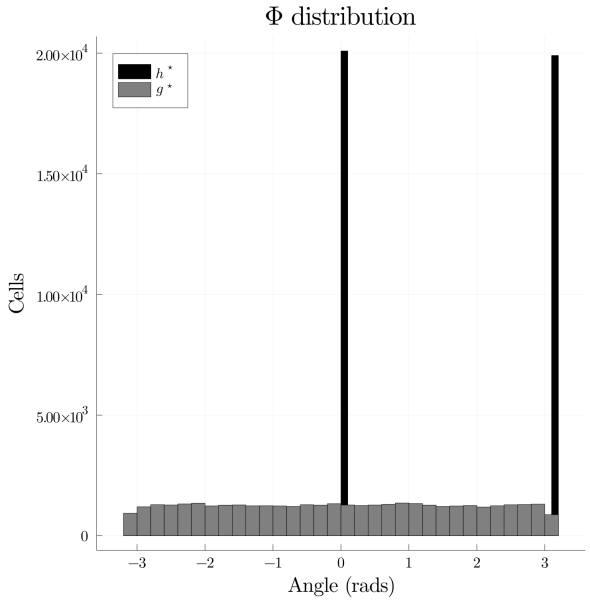

FIG. 10. Distribution of $\phi g^\star$ and $\phi h^\star$ from figures 6 and 9 respectively. Quite visibly, $h^\star$ is the binary DOE.

The binary level DOE leads to an image which appears as two copies of the target image, one doubly-inverted. This appears as a result of the placed constraints on h when taken in conjunction with the properties of the 2D Fourier-transform. This problem is well-known, and partly results from the nature of the algorithm, or as Fienup put it:

> "Like the fabled donkey that starved to death standing between two bales of hay because it was unable to decide which of the two to eat, the algorithm is not readily able to move farther from the features of either of the twin images, and so it is also prevented from moving closer to one rather than the other."[10]

Exploring potential fixes to this problem is beyond the scope of this paper.

XII. ILLUMINATION AND LOW-FREQUENCY FILTERS

The images so far presented are *not* really physical representations of $|G|$. Rather, they are $|\mathcal{F}\, g^\star|$, an estimation which is agnostic to illumination. However, we can simulate $|G|$ by reintroducing s, the source of illumination, via the relation given in eq. 2. We represent $|s|$ using a matrix of equal size to $g^\star$.

FIG. 11. True $|G_5|$. An image resulting from the same $g^\star$ used in figure 6, but now illuminated by the Gaussian laser profile in figure 3.

The effect of illumination is to frequency-filter the image (low-pass). Frequency here

does not refer to the frequency of light ($1/\lambda$), but instead to how elements of g relate to $|G|$. Because of the nature of $\mathcal{F}$, values of $g(x, y)$ for (x, y) near its center 'contribute' sine waves across (u, v) in the far-field plane that are of low spatial frequency, the 'broad strokes' so to speak. Values of $g(x, y)$ for (x, y) further from its center correspond to higher spatial frequencies in (u, v), creating the finer details of $|G|$. The addition of all sine waves from g creates the completed $|G|$, a process which is synonymous with the Fourier-transform.

To see this more clearly, we can purposefully filter only the lowest frequency contributions from $g^\star$, similar to what is seen in the lower part of figure 8, and form a new object-field, $g^\star_f$. The remaining $g^\star_f$ matrix is filled with zeros, achieving a compressed[2] version of $|\mathcal{F}\, g^\star_f|$, which can be seen in figure 12. The final image in the series is almost indistinguishable from figure 11, a wonderful visual proof of the low-frequency-filtering effect of illumination.

If the profile of the laser, $|s|$, is spatially-extended (large) compared to g, then it is approximately uniform over the field, and $g \propto g\star$.

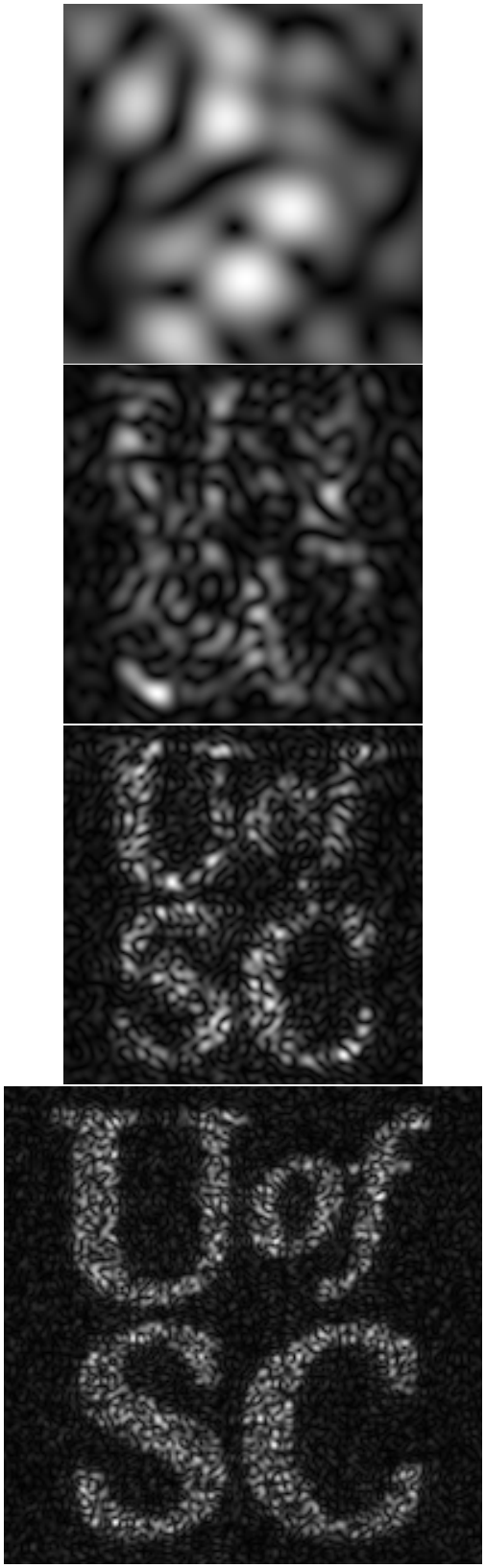

FIG. 12. Each of the above shows $|\mathcal{F}\, g^\star_f|$ created by selecting 36, 400, 1600, 6400 of the lowest frequencies from the $\phi\, g^\star$ of figure 6.

Part IV
Feasibility and Conclusion

XIII. KINOFORM FABRICATION AND NANOFRAZOR CAPABILITIES

A number of factors limit the possibility of fabricating kinoforms on the NanoFrazor.

[2] 'Compressed' because the process of approximating an image by a smaller matrix of its lowest Fourier frequencies constitutes the process of JPEG compression.

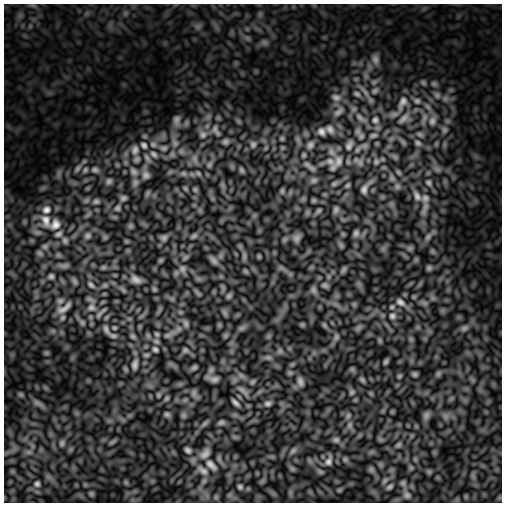

FIG. 13. Look carefully at this $|\mathcal{F}\, g_f^\star|$, and you maybe be able to make out our furry friend from figure 7 using only 6400 of the lowest frequencies.

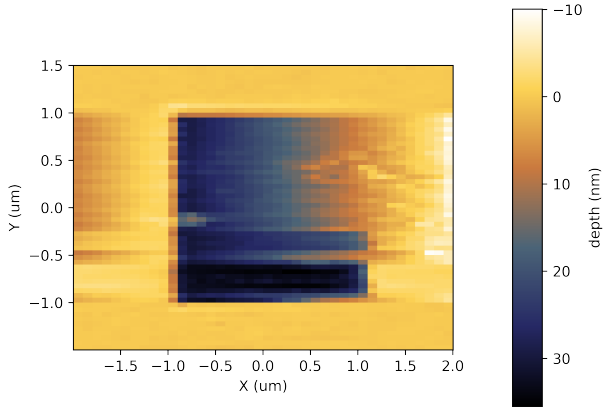

FIG. 14. A test 20×20 field cut onto a $20\,\text{nm} \times 20\,\text{nm}$ section of PPA with the NanoFrazor. Multiple errors and deviations are present. The device is highly sensitive to particularities in the medium's.

The kinoform can never be truly continuous, since it is cut using a digital machine from a digital matrix (proportional to q). The continuity of the kinoform is only achieved when cell density, the number of matrix cells per square micrometer, is high compared to the kinoform depth w, which is likely on the order of half a micrometer. By some estimations, a fresh cutting tip on the NanoFrazor has a diameter of somewhere between 10 nm and 50 nm[11], which puts the maximum cell density at something on the order of 100 to 1000 per nm^2.

In tests on the NanoFrazor, a 400-cell pattern took 30 s to cut. A linear extrapolation implies that a 200×200 resolution pattern such as most of those presented in this paper would take 50 min. The low-frequency approximation in section XII could be used to decrease the fabrication time while maintaining some desired aspects of the image.

XIV. CONCLUSION

For the given system constraints and $|G|$, the q (the kinoform relief) can successfully be determined but not without significant error likely large enough to not be acceptable for high-precision applications. Further investigation is needed into contemporary fixes to the local-optimal solution problem described in section VIII. The binary-DOE condition ought to be the focus of this further study, especially incorporating further constraints posed by nanoparticle self-assembly (e.g. must assemble at magnetic-domain boundaries), and loosening constraints where possible to fully exploit the optical function of the nanoparticles.

Appendix A: Semi-equivalence of Fineup's Algorithm

Fienup recommends that for the next guess, g_{i+1}, for the object-domain field, one uses[12][3]

$$g_{i+1}(x,y) = g_i'(x,y) + \beta \cdot \Delta g_d(x,y), \quad \text{(A1)}$$

where β is a constant "somewhere between 0.5 and 1.0, say 0.7"[13]. Fienup recommends that "For applications requiring the function to have modulus equal to $|f(x,y)|$,

[3] Our variables' conventions are used here instead of Fienup's.

choose[12]:

$$\Delta g_d(x,y) = |f(x,y)| \cdot \frac{g_i'(x,y)}{|g_i'(x,y)|} - g_i'(x,y).$$

For our application, $|f(x,y)| = 1$ for all (x,y). Using an equivalent expression,

$$\Delta g_d(x,y) = |1| \cdot \exp\big(\, \phi\, g_i'(x,y)\big) - g_i'(x,y).$$

Substitution into eq. A1 yields

$$g_{i+1}(x,y) = \beta \cdot \exp \phi\, g_i'(x,y) + (1-\beta) \cdot g_i'(x,y).$$

As Fienup notes, for $\beta = 1$, the equation fully collapses into the Gerchberg-Saxton technique. For other β-values, it is extremely close linear combination between a 1-modulus g_i' and the uncorrected g_i'.

Appendix B: Example NanoFrazor Recipe

The following recipe was used to create the PPA sample used in figure 14:

1. Bathe silicon wafer in Acetone for 2 min.
2. Rinse wafer with IPA.
3. Dry wafer with 30 s of N_2.
4. Bake wafer at 200 °C for 5 min.
5. Place wafer in spin-coater and add 10 drops of PPA.
6. Immediately spin-coat for 1 min at 5, 000 RPM.
7. Bake wafer at 110 °C for 2 min.

[1] L. Ye, T. Pearson, Y. Cordeau, O. T. Mefford, and T. M. Crawford, Triggered self-assembly of magnetic nanoparticles, Scientific Reports **6**, 23145 (2016).

[2] L. B. Lesem, P. M. Hirsch, and J. A. Jordan, The Kinoform: A New Wavefront Reconstruction Device, IBM Journal of Research and Development **13**, 150 (1969).

[3] E. Hecht, *Optics*, 4th ed. (Addison Wesley) p. 540.

[4] R. A. Gonsalves, Phase retrieval from modulus data, JOSA **66**, 961 (1976).

[5] E. Osherovich, Numerical methods for phase retrieval, arXiv:1203.4756 [astro-ph, physics:physics] , 5, 23, 24, 28 (2012), arXiv:1203.4756 [astro-ph, physics:physics].

[6] J. W. Cooley and J. W. Tukey, An algorithm for the machine calculation of complex Fourier series, Mathematics of Computation **19**, 297 (1965).

[7] R. W. Gerchberg and W. Saxton, A Practical Algorithm for the Determination of Phase from Image and Diffraction Plane Pictures, OPTIK **35**, 1 (1971).

[8] J. R. Fienup, Iterative Method Applied To Image Reconstruction And To Computer-Generated Holograms, Optical Engineering **19**, 193297 (1980).

[9] J. R. Fienup, Phase retrieval algorithms: A comparison, Applied Optics **21**, 2758 (1982).

[10] J. R. Fienup and C. C. Wackerman, Phase-retrieval stagnation problems and solutions, JOSA A **3**, 1897 (1986).

[11] NanoFrazor Documentarion Release 3.2.0 (2021).

[12] J. R. Fienup, Reconstruction And Synthesis Applications Of An Iterative Algorithm, in *Transformations in Optical Signal Processing*, Vol. 0373 (SPIE, 1984) pp. 147–160.

[13] J. R. Fienup, Phase retrieval algorithms: A personal tour [Invited], Applied Optics **52**, 45 (2013).